AUT Journal of Electrical Engineering

AUT J. Elec. Eng., 53(1) (2021) 1-10
DOI: 10.22060/eej

Model Predictive Control of a Fault-Tolerant- Hybrid Excitation Axial Field-Flux-Switching Permanent Magnet Motor

S. Jamali Arand[1], J.Rahmani Fard[2]

[1]Electrical Engineering Department, Faculty of Engineering, Yasouj University, Yasouj, Iran
[2] Electrical Engineering Department, Pooyesh Institute of Higher Education, Qom, Iran

ABSTRACT: To improve the performance of the fault-tolerant-hybrid excitation axial field flux-switching (FT-HEAFFS) motor and attain the minimum copper loss, a fault-tolerant control method based on the model predictive control algorithm is proposed. Considering a 6 stator slots/13- rotor poles FT-HEAFFS machine as the control object, under the open circuit failure of single-phase winding, the minimum cropper loss fault-tolerant method based on the model predictive torque control (MPTC) and direct torque control are studied and analyzed, respectively. The feasibility and effectiveness of the proposed fault-tolerant control method are verified. The research results showed that both methods could make the speed, torque and stator flux-linkage almost unchanged, ensuring the stable operation of the system. Compared with direct torque control, the model predictive flux control had smaller flux-linkage ripple before and after the open circuit failure.

Review History:
Received:
Revised:
Accepted:
Available Online:

Keywords:
Hybrid Excited Axial Field Flux-Switching Motor
Model Predictive Torque Control; Direct Torque Control
Open Circuit Fault; Electric Vehicle

1. INTRODUCTION

With the rapid development of science and technology, permanent magnet motors are widely used in electric drive systems of electric vehicles. However, due to the complexity of the control of the electric drive system and the diversity of operating conditions, it is prone to failures, which may cause major accidents in electric vehicles. Therefore, the design of permanent magnet motor drive system with high reliability and high continuity has become a research hotspot of scholars at all around the world [1].

Fault-Tolerant Hybrid Excited Axial Field Flux-Switching (FT-HEAFFS) motor is a new type of doubly salient stator-type permanent magnet motor [2], which combines the advantages flux switching motor and hybrid excitation motor. This motor has compact structure, high power density, high efficiency and strong anti-demagnetization capability. The additional excitation winding makes the air gap magnetic field adjustable, which can increase the output torque and extend the speed range [3-4]. It is suitable for use in the system of frequency conversion and speed regulation of electric vehicles.

The current control strategies of FT-HEAFFS motors are mainly vector control and direct torque control. The vector control recognizes the decoupling of the rotor flux and the electromagnetic torque, which can obtain better steady-state performance, but requires parameter tuning and slow dynamic response [5-6]. Direct torque control does not require rotation coordinate transformation and has a simple structure and fast dynamic response, but is based on the hysteresis control of the flux linkage and torque, which will cause excessive torque and flux linkage pulsation [7-8]. The Model Predictive Torque Control (MPTC) takes torque and stator flux as the control target, and predicts the voltage vector at the next moment by establishing an online loop optimization to minimize the objective function. The MPTC is simple to implement, has fast dynamic response and high tracking accuracy in the field of motor drive and control. It is widely used in [9-12]. In [13-15], the application of MPTC to the control system of the flux-switched permanent magnet motors is proposed. This method has high control accuracy, fast dynamic response, and reduced torque and flux pulsation. Nevertheless, no scholars have conducted in-depth research on MPTC in the field of fault-tolerant control of flux-switched motors. In [16-17], the fault-tolerant control of FT-HEAFFS motor is proposed and a conducted research and analysis on its fault-tolerant control performance is Performed. In [16], the minimum copper loss is taken as the principle and the fault-tolerant control algorithm is driven by solving the relationship between the back electromotive forces. This method can effectively reduce the copper loss before and after the fault, and keep the torque basically stable, but the control algorithm is complex and the control accuracy is not high. [17] studied the space vector pulse width modulation

*Corresponding author's email: email

fault-tolerant control method based on the minimum copper loss. The results show that the control method can achieve the same torque and flux before and after the fault tolerance, but the system response speed is slow.

This paper takes a 6/13-poles FT-HEAFFS motor as the research object and proposes a fault-tolerant control strategy for FT-HEAFFS motor based on MPTC. With considering the mathematical model, and based on the principle of constant magneto-motive force and minimum copper loss for the three-phase four-leg inverter topology, the fault-tolerant control system under DTC and MPTC is simulated and compared to verify the feasibility and superiority of the proposed fault-tolerant control algorithm.

2. THREE-PHASE FT-HEAFFS MOTOR

2.1. Motor structure and working principle

Fig. 1 is a three-dimensional structure diagram of a 6/13 pole FT-HEAFFS motor. The motor consists of two outer stators and an inner rotor with the same structure. Each stator consists of 12 U-shaped conductor cores, 6 permanent magnets, 6 armature windings and 6 field windings. 2 U-shaped conductor cores and 1 permanent magnet form a stator unit and 6 stator units form a stator. The permanent magnets are alternately magnetized in the circumferential direction.

The rotor has 13 cogs, which are evenly placed on the outer circumference of the non-magnetically conductive ring, with neither permanent magnets nor windings. The excitation winding placed in the isolation slot, forms an independent excitation circuit. When the electric drive system fails, the excitation winding can realize fault-tolerant control.

Fig. 2(a) is the working principle diagram of the FT-HEAFFS motor without excitation. The magnetization directions of permanent magnets in two stators are opposite. The 6 armature coils of the stator are divided into three phases, and the two armature coils opposite to each other are connected in series to form a phase. When the rotor cogs move to the U-shaped core c1 and c1' positions, the magnetic flux in the coil reaches the maximum value in the direction indicated by the arrow. When the rotor cogs continue to move to the positions of the U-shaped cores c2 and c2', the magnetic flux in the coil reaches the maximum value in the arrow direction between c2 and c2', and the magnetic flux switching is realized. Fig. 2(b) and (c) are the working principle diagrams of FT-HEAFFS motor during hybrid excitation. The solid line and the dashed line represent the magnetic flux path generated by permanent magnet excitation and DC excitation winding, respectively. In Fig. 2(b), the composite magnetic flux of each phase of the stator winding is strengthened to achieve increased magnetization. In Fig. 2(c), the composite magnetic flux of the stator winding is weakened to achieve magnetic weakening.

2.2. Mathematical model

Using the traditional permanent magnet synchronous motor (PMSM) modeling analysis method, the mathematical model of the FT-HEAFFS motor in the d-q coordinate system is obtained. The basic equation is as follows:

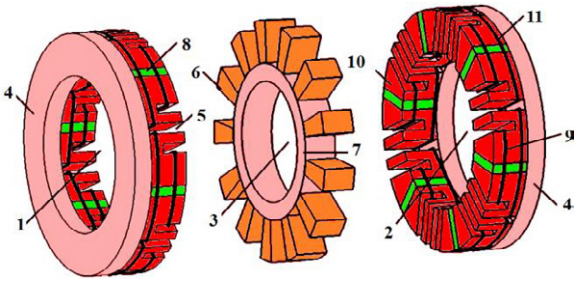

Fig. 1. 1-stator 1, 2-stator 2, 3-rotor, 4-non-magnetic fixed disk, 5-isolation slot, 6-rotor pole, 7-non-magnetic material, 8-permanent magnet, 9-armature winding, 10-U-shaped iron core, 11-excitation winding

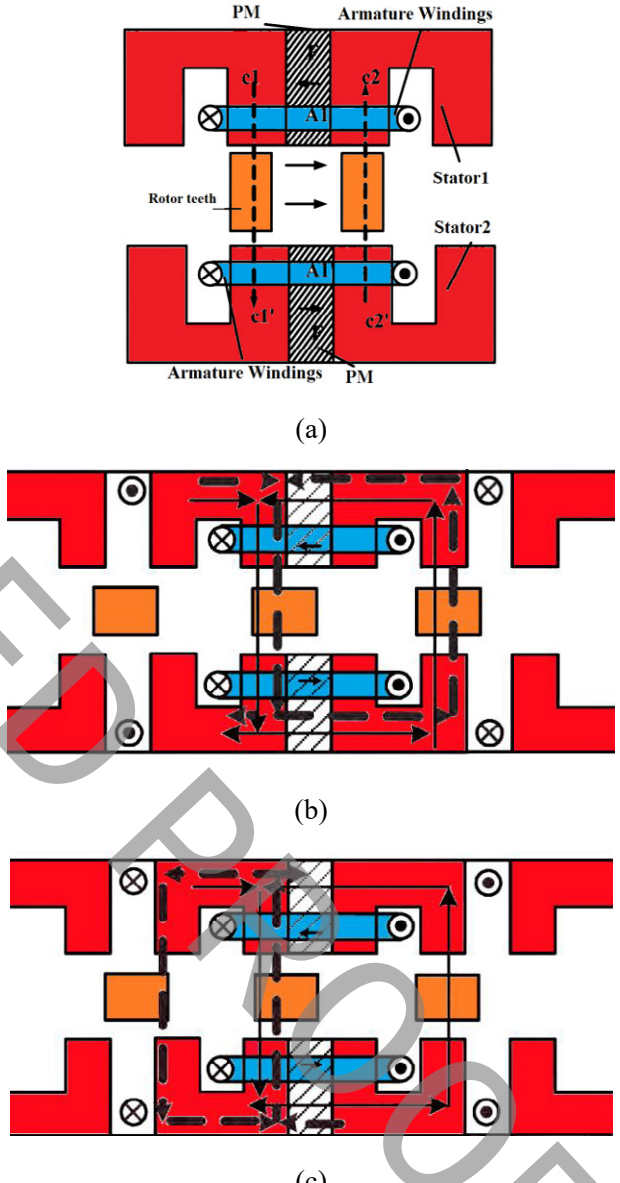

Fig.2. FT-HEAFFS motor working principle. (a) Without excitation. (b) Promagnetization. (c) Demagnetization.

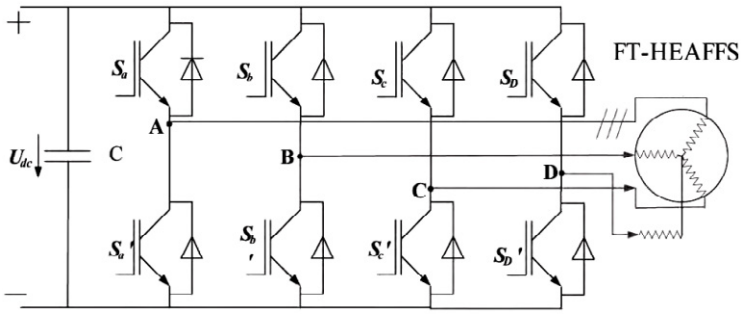

Fig.3. Three-phase four-leg fault-tolerant inverter topology

$$\begin{cases} \psi_{\mathrm{d}} = L_{\mathrm{d}} i_{\mathrm{d}} + M_{sf} i_f + \psi_{\mathrm{pm}} \\ \psi_{\mathrm{q}} = L_{\mathrm{q}} i_{\mathrm{q}} \\ \psi_{\mathrm{f}} = L_{\mathrm{f}} i_{\mathrm{f}} + \dfrac{3}{2} M_{sf} i_f + + \psi_{\mathrm{pmf}} \end{cases} \quad (1)$$

The voltage equations are as follows

$$\begin{cases} u_{\mathrm{d}} = L_{\mathrm{d}} \dfrac{\mathrm{d}i_{\mathrm{d}}}{\mathrm{d}t} + M_{sf} \dfrac{di_f}{dt} - \omega_{\mathrm{r}} L_{\mathrm{q}} i_{\mathrm{q}} + R_{\mathrm{s}} i_{\mathrm{d}} \\ u_{\mathrm{q}} = L_{\mathrm{q}} \dfrac{\mathrm{d}i_{\mathrm{q}}}{\mathrm{d}t} + \omega_{\mathrm{r}} \left(L_{\mathrm{d}} i_{\mathrm{d}} + M_{sf} i_f + \psi_{\mathrm{pm}} \right) + R_{\mathrm{s}} i_{\mathrm{q}} \\ u_{\mathrm{f}} = R_{\mathrm{f}} i_{\mathrm{f}} + \dfrac{3}{2} M_{sf} \dfrac{\mathrm{d}i_{\mathrm{d}}}{\mathrm{d}t} + L_{\mathrm{f}} \dfrac{\mathrm{d}i_{\mathrm{f}}}{\mathrm{d}t} \end{cases} \quad (2)$$

The electromagnetic torque and motion equations can express as

$$T_{\mathrm{e}} = \frac{3}{2} \mathrm{p} \psi_{\mathrm{pm}} i_{\mathrm{q}} + \frac{3}{2} \mathrm{p} \left(L_{\mathrm{q}} - L_{\mathrm{d}} \right) i_{\mathrm{d}} i_{\mathrm{q}} + \frac{3}{2} \mathrm{p} M_{sf} i_f i_q \quad (3)$$

$$T_{\mathrm{e}} - T_{\mathrm{l}} = \frac{J}{p} \frac{d\omega_{\mathrm{r}}}{dt} + B\omega_{\mathrm{r}} \quad (4)$$

In the equations, R_s and R_f are stator resistance and field winding resistance, respectively. L_d, L_q, L_f are the d -q axes armature inductances and magnetizing inductance. i_d, i_q and i_f are d -q axes armature current and excitation current. u_d, u_q, u_f, are d -q axes armature voltage and excitation voltage. ψ_d,, ψ_q,, ψ_{pm}, ψ_{pmf} are d -q axes flux linkage, the permanent magnet flux linkage and the flux linkage in the excitation winding. M_{sf} is the mutual inductance between the phase winding and the field winding. T_l, is load torque, ω_r is the mechanical angular velocity, p is the number of pole pairs, J is the moment of inertia and B is the coefficient of friction.

3. FT-HEAFFS MOTOR CONTROL STRATEGY

Single-phase winding open circuit fault is one of the main faults of three-phase motors. In this paper, the fault-tolerant control of DTC and MPTC of the three-phase 6/13 FT-HEAFFS motor is studied and compared to the single-phase winding open circuit fault.

3.1. Fault-tolerant control algorithm

When the FT-HEAFFS motor is running normally, the armature rotating magneto-motive force formed by the three-phase symmetrical current of the stator is circular. When the single-phase winding is open-circuited, the magneto-motive force becomes elliptical due to the asymmetry of the winding, which causes the output torque of the motor to produce large pulsations. Using the constant magneto-motive force method can ensure that the force remains round and unchanged before and after the single-phase winding open-circuit fault, and the stable operation of the motor is ensured. The phase current of the three-phase winding during normal operation is:

$$\begin{cases} i_a = I_m \cos\left(\omega_e t\right) \\ i_b = I_m \cos\left(\omega_e t - \dfrac{2}{3}\pi\right) \\ i_c = I_m \cos\left(\omega_e t + \dfrac{2}{3}\pi\right) \end{cases} \quad (5)$$

The three-phase rotating magneto-motive force generated by the three-phase winding phase current is as:

$$\begin{cases} F_a = N i_a \\ F_b = N i_b \\ F_c = N i_c \end{cases} \quad (6)$$

From equations (5)-(6), the magneto-motive force can express as

$$\sum F = F_a + aF_b + a^2 F_c = \frac{3}{2} N I_m \left(\cos\theta_e + j \sin\theta_e \right) \quad (7)$$

Where I_m is the amplitude of the phase current, N is the number of turns of each phase in series and $\alpha = 1\angle 120°$.

Fig. 3 shows the topology of the three-phase four-leg

Table 1. The voltage vector table of FT-HEAFFS motor in normal operation

	U_{AN}	U_{BN}	U_{CN}	U_{α}	U_{β}
000	0	0	0	0	0
001	$-\frac{1}{3}U_{dc}$	$-\frac{1}{3}U_{dc}$	$\frac{2}{3}U_{dc}$	$-\frac{1}{3}U_{dc}$	$-\frac{1}{\sqrt{3}}U_{dc}$
010	$-\frac{1}{3}U_{dc}$	$\frac{2}{3}U_{dc}$	$-\frac{1}{3}U_{dc}$	$-\frac{1}{3}U_{dc}$	$\frac{1}{\sqrt{3}}U_{dc}$
011	$-\frac{2}{3}U_{dc}$	$\frac{1}{3}U_{dc}$	$\frac{1}{3}U_{dc}$	$-\frac{2}{3}U_{dc}$	0
100	$\frac{2}{3}U_{dc}$	$-\frac{1}{3}U_{dc}$	$-\frac{1}{3}U_{dc}$	$\frac{2}{3}U_{dc}$	0
101	$\frac{1}{3}U_{dc}$	$-\frac{2}{3}U_{dc}$	$\frac{1}{3}U_{dc}$	$\frac{1}{3}U_{dc}$	$-\frac{1}{\sqrt{3}}U_{dc}$
110	$\frac{1}{3}U_{dc}$	$\frac{1}{3}U_{dc}$	$-\frac{2}{3}U_{dc}$	$\frac{1}{3}U_{dc}$	$\frac{1}{\sqrt{3}}U_{dc}$
111	0	0	0	0	0

fault-tolerant inverter. When the A-phase winding fails, it will be removed and the D-phase bridge arm will be connected. The D-phase and the non-faulty phases form a new three-leg structure. The three-phase current of the motor under fault-tolerant operation is:

$$\begin{cases} i_a = 0 \\ i_b = I'_m \cos\left(\omega_e t - \frac{2}{3}\pi + \theta_B\right) \\ i_c = I'_m \cos\left(\omega_e t + \frac{2}{3}\pi + \theta_C\right) \end{cases} \quad (8)$$

Where, I'_m is the non-fault phase current amplitude after the open circuit fault, θ_B and θ_C are the angle phase change values of the B and C phase currents, respectively. At this time, the magneto-motive force ($\Sigma F'$) is calculated similar to equation (7).

Let $\Sigma F = \Sigma F'$. This yields θ_B=-30°, θ_C=30°, $I'_m = \sqrt{3}\ I_m$. By substituting these values into equation (8), we have

$$\begin{cases} i_a = 0 \\ i_b = \sqrt{3} I_m \cos\left(\omega_e t - \frac{5}{6}\pi\right) \\ i_c = \sqrt{3} I_m \cos\left(\omega_e t + \frac{5}{6}\pi\right) \end{cases} \quad (9)$$

It can be seen from equations (5) and (9) that the non-fault phase current after fault tolerance is $\sqrt{3}$ times of normal operation. When the load is heavy, it is easy to cause secondary faults and serious damages to the motor. When the motor is under the open circuit fault and fault-tolerant operation, the field winding can increase the magnetization to reduce the amplitude of the non-fault phase current. When the FT-HEAFFS motor is running normally, the inverter works in three-phase full-bridge mode, and the phase voltage values are synthesized by the eight space voltage vectors (000~111). The phase voltage value synthesized under the αβ0 coordinate system is shown in Table 1.

In this Table, U_{AN}, U_{BN} and U_{CN} are the voltage values between the three phases of A, B, and C and the neutral point of the winding, and U_{α} and U_{β} are the voltage values of U_{AN}, U_{BN} and U_{CN} after Clark transformation.

When the FT-HEAFFS motor has a single-phase fault, the system cuts off the faulty phase, and the inverter switches to the two-phase three-leg working mode. For example, take the A-phase as faulty phase, use the fourth bridge arm D-phase instead of the faulty phase A to generate the space voltage vector. The original PWM drive signal that controls the A-phase bridge arm switches is used to control the D-phase bridge arm switches. The voltage vector Table during fault-tolerant operation is shown in Table 2.

In this Table, U_{DN}, U_{BN} and U_{CN} are the voltage values between the three phases of D, B, and C and the neutral point of the winding, and U_{α} and U_{β} are the voltage values of U_{DN}, U_{BN} and U_{CN} after Clark transformation.

This paper takes the minimum copper loss of the motor as the optimization goal, and proposes a fault-tolerant control method of the minimum copper loss combined with the adjustment of the excitation current.

The copper loss before and after the fault tolerance of AFFSFT motors can be calculated as follows:

(1) Copper loss during the normal operation of the motor can express as

$$P_{copper} = 3I_s^2 R_s \quad (10)$$

Table 2. The voltage vector table of FT-HEAFFS motor during fault-tolerant operation

	U_{DN}	U_{BN}	U_{CN}	U_α	U_β
000	0	0	0	0	0
001	0	0	U_{dc}	$-\frac{1}{3}U_{dc}$	$-\frac{1}{\sqrt{3}}U_{dc}$
010	0	U_{dc}	0	$-\frac{1}{3}U_{dc}$	$\frac{1}{\sqrt{3}}U_{dc}$
011	0	U_{dc}	U_{dc}	$-\frac{2}{3}U_{dc}$	0
100	0	$-U_{dc}$	$-U_{dc}$	$\frac{2}{3}U_{dc}$	0
101	0	$-U_{dc}$	0	$\frac{1}{3}U_{dc}$	$-\frac{1}{\sqrt{3}}U_{dc}$
110	0	0	$-U_{dc}$	$\frac{1}{3}U_{dc}$	$\frac{1}{\sqrt{3}}U_{dc}$
111	0	0	0	0	0

Table 3. excitation current and back-EMF at rated speed

Excitation current i (A)	Back-EMF (V)	Per unit back-EMF	$Pv(i_f)$
0	27.2	1	1
1	29.6	1.088235294	1.088235294
3	32.0	1.176470588	1.176470588
4	33.6	1.235294118	1.235294118

I_s is the effective value of the single-phase armature winding current.

(2) The copper loss during the fault-tolerant operation of the motor can express as (without using the field winding to increase magnetization):

$$P_{copper} = 2\left(\sqrt{3}I_s\right)^2 R_s = 6I_s^2 R_s \tag{11}$$

(3) The copper loss during the fault-tolerant operation of the motor is (using the field winding to increase the magnetization):

$$\begin{aligned} P_{copper} &= i_f^2 R_f + 2\left[\sqrt{3}\frac{\psi_{pm}}{\psi_{pm}Pv\left(i_f\right)}I_s\right]^2 \\ R_s &= i_f^2 R_f + \frac{6I_s^2 R_s}{Pv^2\left(i_f\right)} \end{aligned} \tag{12}$$

In the formula, $\psi_{pm}Pv\left(i_f\right)$ is the function of the amplitude of the phase permanent magnet flux linkage when field winding is used to increase the magnetization. Since the Back-EMF increases by $Pv\left(i_f\right)$ times, the current must be reduced by $Pv\left(i_f\right)$ times to create the same power.

The numerical expression of the function $Pv(i_f)$ can be obtained through finite element software simulation or experiment. This article uses the experimental method for measuring. When the motor runs stably at the rated speed n=200r/min, the data shown in Table 3 is obtained. Take the back-EMF amplitude at i_f=0 as the basic value to normalize the back-EMF data. Due to the limitation of the experimental conditions, only the data that the amplitude of the permanent magnet flux linkage of the motor phase increases with the excitation current is measured. There is no data to measure the demagnetization of the amplitude of the motor phase permanent magnet flux with the excitation current. Therefore, there will be a certain error in the subsequent calculation of the optimal excitation current and the theoretical value. But it does not affect the correctness and feasibility of the copper loss minimization optimization algorithm.

Through fitting, $Pv(i_f)$ can be expressed as

$$Pv\left(i_f\right) = 1.251 - 0.2507e^{-0.5533i_f} \tag{13}$$

It can be determined that after using the field winding to assist fault tolerance, the copper loss during fault-tolerant operation of the motor has a minimum value as it increases. For different effective values of armature current, the optimal excitation current distribution diagram can be obtained, as shown in Fig. 4, and the small circle on the curve is the minimum point.

By substituting equation (13) into (12), the optimal

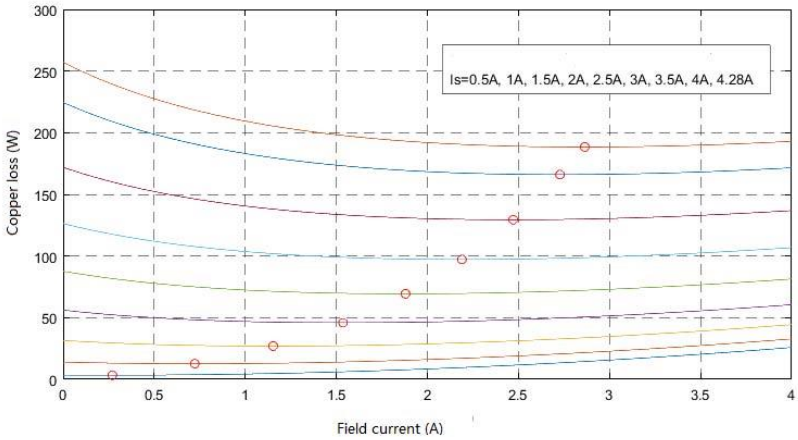

Fig. 4. The distribution diagram of the excitation current with minimum copper loss

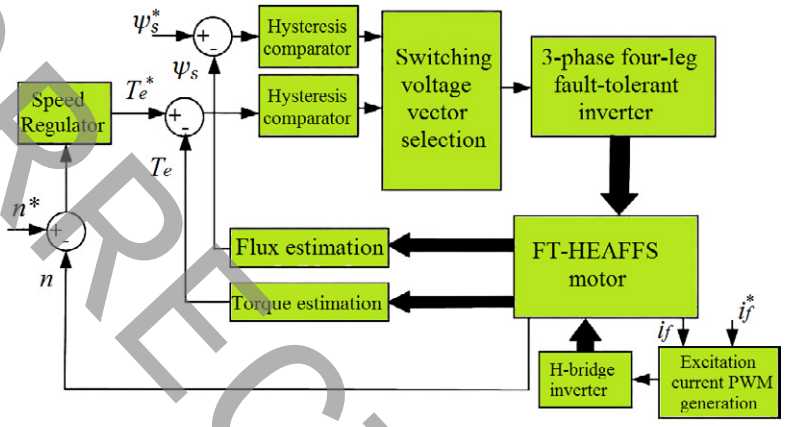

Fig.5. Block diagram of the motor fault-tolerant control system based on DTC algorithm

excitation current is obtained, and the non-fault phase stator currents amplitude can be minimized by adjusting the optimal excitation current, and the copper loss of the system can be reduced.

3.2. Direct torque control (DTC)

DTC does not need rotating coordinate transformation, current inner loop and PWM link, and has the advantages of simple structure and fast dynamic response. Applying DTC to the fault-tolerant control of FT-HEAFFS motor, better dynamic performance is achieved. The fault-tolerant control block diagram of FT-HEAFFS motor based on DTC algorithm is shown in Fig. 5. The FT-HEAFFS motor control system mainly includes 6 modules: 1-speed loop control module, 2-flux linkage and torque Bang-Bang control module, 3-flux linkage estimation and torque calculation module, 4-switching voltage vector selection module, 5-three-phase four-leg fault-tolerant inverter and H-bridge inverter module 6-excitation current PWM generation module.

The given speed and the actual measured speed compared in speed regulator and the reference torque is the output of the speed regulator and is the input of the torque loop. The flux reference value ψ_s^* remains at the rated value (0.05Wb) and the output of the speed proportional-integral (PI) controller is defined as the given electromagnetic torque T_e^*. The reference torque and flux linkage are respectively compared with the values calculated by the torque and flux linkage calculation module in real time, and then sent to the hysteresis comparator to determine the switching voltage vector according to the output result to control the on-off of the fault-tolerant inverter.

When the A-phase open-circuit fault occurs, the A-phase switching value is switched to the D-phase to realize the fault-tolerant control of the motor. At the same time, by adjusting the optimal excitation current, the non-fault phase stator current amplitude can be minimized, and the copper loss of the control system can be reduced.

3.3. Model Predictive Torque Control

MPTC is different from the DTC online look-up Table control method. This control method selects the optimal voltage vector based on the value function by evaluating the torque and flux linkage of each sampling period, while selecting the voltage vector corresponding to the minimum of value function. This method does not require complex PWM modulation, has a simple algorithm, is suitable for processing nonlinear factors, has good restraint ability, can effectively reduce the ripple of torque and flux linkage, and improves the

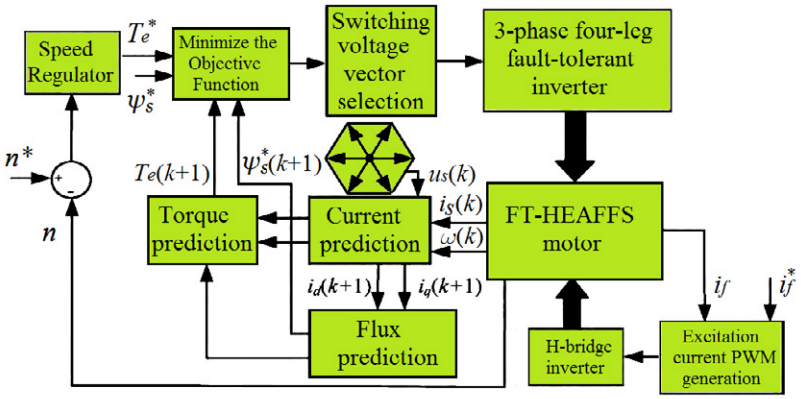

Fig. 6. Block diagram of the motor fault-tolerant control system based on MPTC

Table 4. FT-HEAFFS motor parameters

Parameter	value	Parameter	value
Phase resistance/Ω	2.4	Permanent magnet flux/Wb	0.1
Phase winding self-inductance/mH	18.75	Moment of inertia/(kg·m²)	0.0008
Phase winding mutual inductance/mH	2.44	Coefficient of friction	0.00001
Field winding resistance/Ω	1.52	d- axis inductance id/mH	0.0063
Self-inductance of field winding/mH	5.28	q- axis inductance iq/mH	0.0065
Winding leakage inductance/mH	1	Rated power/W	600

dynamic response performance of the motor. The structure diagram of the FT-HEAFFS motor based on proposed MPTC is shown in Fig. 6.

The current prediction model obtained by Euler discretization of u_d and u_q can express as:

$$\begin{cases} i_d(k+1)=\left(1-\dfrac{R_sT_s}{L_d}\right)i_d(k)+ \\ \omega_e(k)T_s\dfrac{L_q}{L_d}i_q(k)+\dfrac{T_s}{L_d}u_{sd}(k) \\ i_q(k+1)=-\omega_e(k)T_s\dfrac{L_d}{L_q}i_d(k)+ \\ \left(1-\dfrac{R_sT_s}{L_q}\right)i_q(k) \\ +\dfrac{T_s}{L_q}u_{sq}(k)-\dfrac{\omega_eT_s\left(\psi_{pm}+M_{sf}i_f\right)}{L_q} \end{cases} \tag{14}$$

where, *Ts* is the sampling period, and *k* and *k*+1 are the sampling at k and k+1 period, respectively. Substituting Equation (14) into Equation (1), the stator flux linkage prediction model can be obtained as :

$$\begin{cases} \psi_{sd}(k+1)=L_di_d(k+1)+M_{sf}i_f+\psi_{pm} \\ \psi_{sq}(k+1)=L_qi_q(k+1) \end{cases} \tag{15}$$

Substituting Equation (14) into Equation (3), the torque prediction model can be obtained as:

$$\begin{aligned} T_e(k+1)&=\frac{3}{2}\mathrm{p}i_q(k+1) \\ &\left(\psi_{\mathrm{pm}}+\left(L_q-L_d\right)i_d(k+1)+M_{sf}i_f\right) \end{aligned} \tag{16}$$

The objective function is defined as:

$$G=\left|T_e(k+1)-T_e^*\right|+\lambda\left|\psi_s(k+1)-\psi_s^*\right| \tag{17}$$

where, T_e^* and ψ_s^* are the reference values of torque and flux linkage respectively, and λ is the weight coefficient.

4. SYSTEM SIMULATION

In order to verify the control performance of the proposed MPTC-based FT-HEAFFS motor fault-tolerant control strategy, this paper builds the MPTC and DTC control system simulation models of the motor in Simulink/ Matlab, and conducts a simulation comparison study on its dynamic and

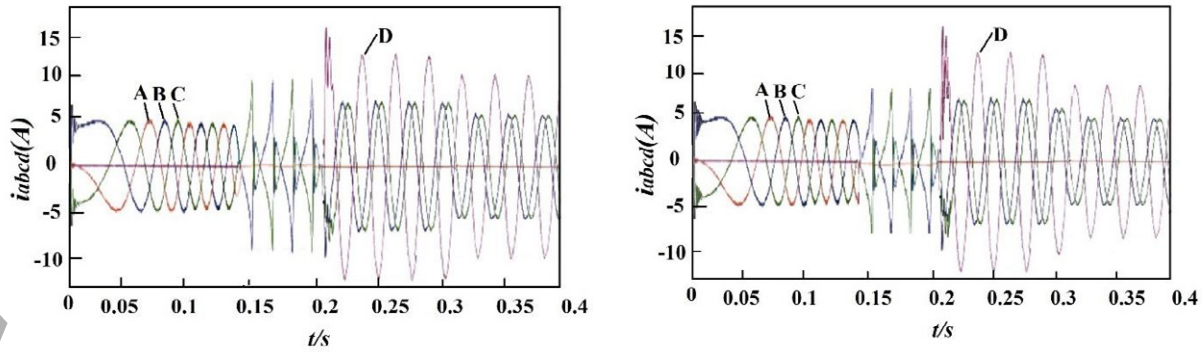

(a) (b)

Fig. 7. Three-phase current waveforms. (a) DTC strategy. (b) MPTC strategy

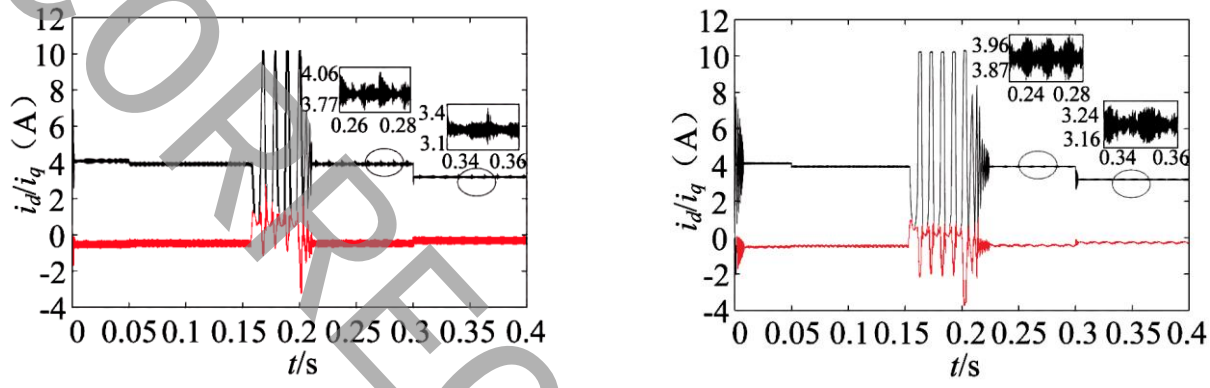

(a) (b)

Fig. 8. Current waveform of d-q axes. (a) DTC strategy. (b) MPTC strategy

steady-state performance and fault-tolerant control effect. In the FT-HEAFFS motor simulation system, the parameter setting of the motor directly affects the final simulation result. This paper combines the experimental prototype parameters and the finite element simulation results to set the motor model parameters as shown in Table 4.

Figs 6 to 8 are the simulation waveforms of fault-tolerant control systems based on DTC and MPTC. The speed is set to 200 r/min, the load torque reference value is always 7.6 N.m, the excitation current (i_f) is 0.3335 A, and the weight coefficient λ is 300. At 0~0.05 s, the motor starts and the speed rises steadily to 200 r/min; at 0.05~0.15 s, the motor runs stably at a speed of 200 r/min; at 0.15 s, in phase A, an open circuit fault occurs and runs at 0.15~0.2 s. The fault-tolerant control without excitation runs at 0.2 s, and lasts up to 0.3 s. The excitation current is added at 0.3 s, and the fault-tolerant operation with the smallest copper loss is realized at 0.3~0.4 s. In 0~0.4 s, the DTC and MPTC control strategies were simulated and compared for the motor drive system under different working conditions.

Fig. 7 shows the three-phase current waveforms under the DTC and MPTC control strategies. It can be seen that the control effects of the two strategies are basically the same. When the motor fails, without the excitation fault-tolerant control, the amplitude of phase A is 0, phase B and phase C become $\sqrt{3}$ times of the normal operation and the phase angle deflection by ±30°. Phase D replaces with the removed faulty phase, and rebalances with the phase B and C currents. The results are consistent with the theoretical analysis; during the minimum copper loss fault-tolerant control, the normal phase current amplitude is reduced from 6.9A to 5.6A, a decrease of 18.8%.

Fig. 8 shows the current waveforms of the d-q axes under the two control strategies. With taking the d-axis current ripple as an example: when the fault-tolerant control is performed without excitation, the d-axis current of the FT-HEAFFS motor under the DTC control strategy fluctuates between 3.77~4.06 A and under the MPTC control strategy fluctuates between 3.87~3.96 A. Later, the current ripple is reduced by 68.7٪ . When the fault-tolerant operation runs with the smallest copper loss, the d-axis current ripple rate under the DTC control strategy is 10.1%, and under the MPTC control strategy is 2.5%, this means that the current ripple is significantly reduced.

Figs 9-11 show the speed, flux linkage and torque waveforms respectively. The speed and flux linkage under the

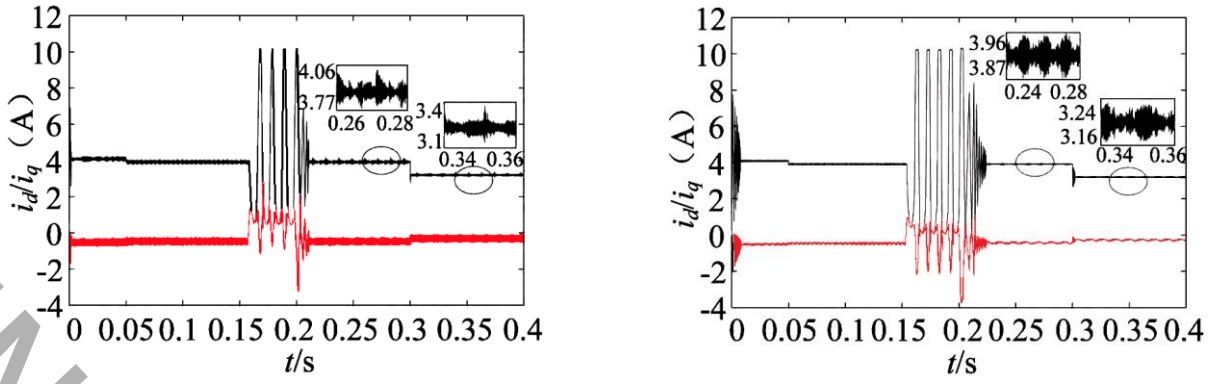

(a) (b)

Fig. 9. Speed waveform. (a) DTC strategy. (b) MPTC strategy

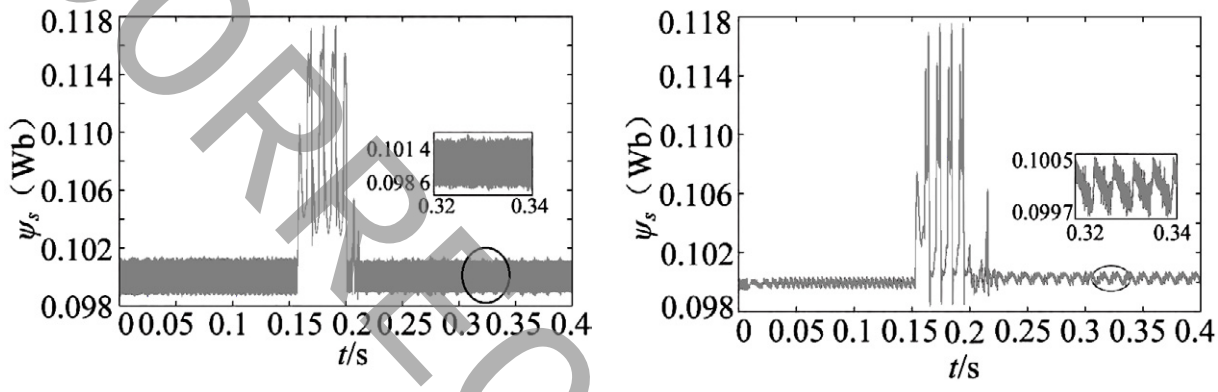

(a) (b)

Fig. 10. Flux linkage waveform. (a) DTC strategy. (b) MPTC strategy

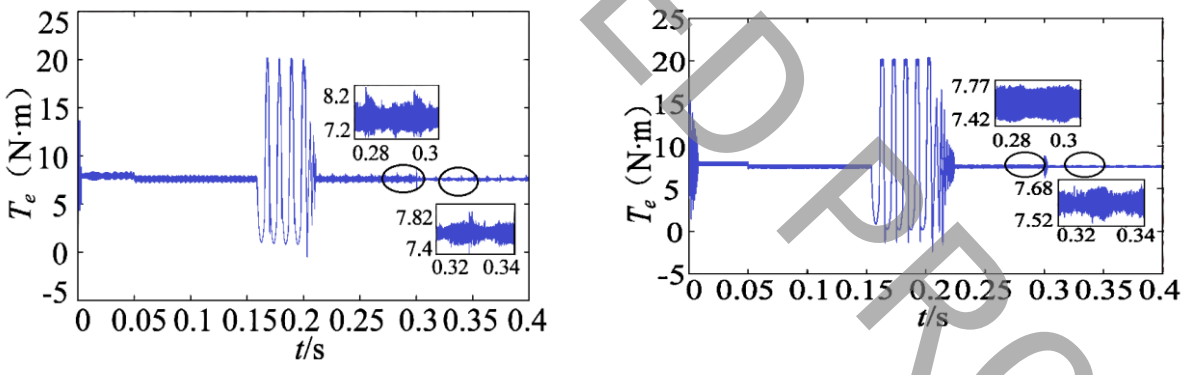

(a) (b)

Fig. 11. Torque. (a) DTC strategy. (b) MPTC strategy.

two control strategies can quickly keep up with the reference value before and after the fault, and the overshoot is small. In the stage of fault-tolerant operation without excitation, the flux linkage and torque ripple under MPTC control strategy are 0.8% and 4.6%, respectively, and the ripples under DTC control strategy are 2.8% and 13%. In the stage of fault-tolerant operation with minimum copper loss, the torque ripple under the MPTC control strategy is significantly reduced, with a ripple rate of only 2.2%, which is 60% lower than that of the DTC control strategy. It can be seen from the Figs, that the MPTC-based fault-tolerant control strategy has a significant effect on the improvement of motor torque and flux ripple.

Table 5. Comparison of the results

Parameter	DTC strategy	MPTC strategy
d-axis current ripple (In fault-tolerant operation without excitation)	12.1%.	3.84%
d-axis current ripple (In fault-tolerant operation with minimum copper loss)	10.1%,	2.5%,
Flux linkage ripple (In fault-tolerant operation without excitation)	4.6%	0.8%
Torque ripple (In fault-tolerant operation without excitation)	13%.	2.8%
Torque ripple (In fault-tolerant operation with minimum copper loss)	3.66%	2.2%,

For better comparison, the results are listed in Table 5.

5. CONCLUSION

This paper studies and analyzes the fault-tolerant control strategy based on the MPTC and the DTC for a new three-phase 6/13 pole FT-HEAFFS motor. A single-phase open-circuit fault-tolerant control system under two control strategies is built, simulated and compared. The research results show that: the two fault-tolerant control strategies both enable the motor torque and stator flux linkage after fault tolerant to reach the control effect approximately in normal operation. Using the fault-tolerant optimization algorithm with the least copper loss can effectively reduce the phase current amplitude, thereby reducing the motor loss after a fault. Compared with the DTC fault-tolerant control strategy, the motor torque and stator flux pulsation under the MPTC fault-tolerant control strategy are significantly reduced, which improves the steady-state performance of the motor during fault operation.

REFERENCES

[1] X. Dianguo, B. Wang, G. Zhang, G. Wang, and Y. Yu. "A review of sensorless control methods for AC motor drives." CES Transactions on electrical machines and systems, vol. 2, no. 1, pp. 104-115, 2018.

[2] A. Metin, S. Huang, T. A. Lipo. "Design, analysis, and control of a hybrid field-controlled axial-flux permanent-magnet motor" IEEE Transactions on industrial electronics, vol. 57, no. 1, pp. 78-87, 2009.

[3] D. Wang, S. Chunlei, and W. Xiuhe. "Investigation of a novel hybrid radial and axial magnetic circuit permanent magnet motor with flux weakening capability for EVs." In 2017 20th International Conference on Electrical Machines and Systems (ICEMS), pp. 1-6. IEEE, 2017.

[4] Zhang W, Liang X, Lin M, et al. "Design and Analysis of Novel Hybrid-Excited Axial Field Flux-Switching Permanent Magnet Machines." IEEE Transactions on Applied Superconductivity, vol. 26, no. 4, pp.1-5, 2016.

[5] Z. Zhang, Y. Liu, B. Tian, W. Wang, "Investigation and implementation of a new hybrid excitation synchronous machine drive system." IET Electric Power Applications, vol.11, no. 4, pp.487-494, 2017.

[6] J. Sawma, F. Khatounian, E. Monmasson, L. Idkhajine, R. Ghosn, "Analysis of the impact of online identification on model predictive current control applied to permanent magnet synchronous motors." IET Electric Power Applications, vol. 11, no.5, pp.864-873, 2017.

[7] Y. Wang, , Z. Deng, X. Wang, "A parallel hybrid excitation flux-switching generator DC power system based on direct torque linear control. IEEE Transactions on Energy Conversion, vol. 27, no. 2, pp.308-317, 2012.

[8] X.Yuan, W. Zhang, X. Liang, L.Hao, Y. Liang, "Research of Control Methods for Axial Field Flux-Switching Permanent Magnet Machine". In 2018 21st International Conference on Electrical Machines and Systems (ICEMS), pp. 1218-1222. IEEE 2018.

[9] H. Miranda, P. Cortes, J. I. Yuz, et al. "Predictive Torque Control of Induction Machines Based on State-Space Models" IEEE Transactions on Industrial Electronics, vol. 56, no. 6, pp. 1916-1924, 2009.

[10] T. Wang, "Model predictive control of electromagnetic torque in permanent magnet synchronous machines." PhD diss., 2013.

[11] J.Rahmani Fard, M. Ardebili, "Sensor-less control of a novel axial flux-switching permanent-magnet motor", COMPEL - The international journal for computation and mathematics in electrical and electronic engineering, Vol. 37, no. 6, pp. 2299-2312, 2018.

[12] T. Geyer, "Model predictive control of high power converters and industrial drives". John Wiley & Sons, 2018.

[13] W. Huang, W. Hua, F. Chen, F. Yin, J. Qi,. "Model predictive current control of open-circuit fault-tolerant five-phase flux-switching permanent magnet motor drives." IEEE Journal of Emerging and Selected Topics in Power Electronics, vol. 6, no. 4, pp.1840-1849, 2018.

[14] Z. Chen, X.D. Liu, Y.Q. Jin, Y.P. Dai, "Direct torque control of permanent magnet synchronous motors based on extended Kalman filter observer of flux linkage", Proceedings of the CSEE, 33, 2008.

[15] S. Hanke, O. Wallscheid, J. Böcker, "A direct model predictive torque control approach to meet torque and loss objectives simultaneously in permanent magnet synchronous motor applications." In 2017 IEEE International Symposium on Predictive Control of Electrical Drives and Power Electronics (PRECEDE), pp. 101-106, IEEE 2017.

[16] J. Yu, P. Shi, W. Dong, B. Chen, C. Lin, "Neural network-based adaptive dynamic surface control for permanent magnet synchronous motors." IEEE transactions on neural networks and learning systems, vol. 26, no. 3, pp. 640-645, 2014.

[17] F.J. Lin, J.C. Hwang, P.H. Chou, Y.C. Hung, "FPGA-based intelligent-complementary sliding-mode control for PMLSM servo-drive system." IEEE transactions on power electronics, vol. 25, no. 10, pp. 2573-2587, 2010.

[18] W. Zhang, X. Liang, F. Yu, "Fault-Tolerant Control of Hybrid Excitation Axial Field Flux-Switching Permanent Magnet Machines", IEEE Transactions on Magnetics, vol. 54, no. 11, pp. 1-5, 2018.

HOW TO CITE THIS ARTICLE

Jamali Arand, S., Rahmani Fard, J. (2021). Model Predictive Control of a Fault-Tolerant-Hybrid Excitation Axial Field-Flux-Switching Permanent Magnet Motor. AUT J. Elec. Eng., 53(1): 1-10.

DOI: 10.22060/eej***